# Understanding the Origins of Changing the Product Specificity Properties of Arginine Methyltransferase PRMT7 by E181→D and E181→D/Q329→A Mutations: A QM/MM Study

Wan-Sheng Ren[ǂ,1], Adua Rahman[ǂ,2], Kai-Bin Jiang[ǂ,1,‡], Hao Deng[1], Yuan-Yuan Zhao[1], Wei-Jie Zhang[1], Kedian Liu[2], Ping Qian,[*,1] and Hong Guo[*,2]

[1] *Chemistry and Material Science Faculty, Shandong Agricultural University, Taian 271018, P. R. China*

[2] *Department of Biochemistry and Cellular and Molecular Biology, University of Tennessee, Knoxville, TN 37996, United States UT/ORNL Center for Molecular Biophysics, Oak Ridge National Laboratory, Oak Ridge, TN 37830, United States*

[ǂ] These authors contributed equally to this work.

[‡] Current Address: State Key Laboratory of Structural Chemistry, Fujian Institute of Research on the Structure of Matter, Chinese Academy of Sciences, 350002, P. R. China.

[*] Corresponding authors: Tel.: +86 538 8241175; fax: +86 538 8242251.

E-mail address: qianp@sdau.edu.cn (to P. Qian) and hguo1@utk.edu (to H. Guo)

# Abstract

Arginine methylations can regulate important biological processes and affect many cellular activities, and the enzymes that catalyze the methylations are protein arginine methyltransferases (PRMTs). The biological consequences of arginine methylations depend on the methylation states of arginine that are determined by the PRMT’s product specificity. Although the product specificity is a very important property, it is still unknown concerning why different PRMTs may generate different methylation states for the target arginine residues on protein substrates. PRMT7 is the only known member of Type III PRMT that produces mono-methylarginine (MMA) product. Interestingly, its E181D and E181D/Q329A mutants can catalyze, respectively, the formation of asymmetrically di-methylated arginine (ω-$N^G$, $N^G$-dimethylarginine or ADMA) and symmetrically di-methylated arginine (ω-$N^G$, $N'^G$-dimethylarginine or SDMA). The exact reasons for such product specificity modification as a result of the mutations have been unclear. Here QM/MM molecular dynamics (MD) and potential of mean force (PMF) free-energy simulations are performed for the E181D and E181D/Q329A mutants to understand the catalytic mechanism and the origin of their different product specificities from that of the wild-type PRMT7 as well as between E181D and E181D/Q329A. The simulations show that while the free energy barriers of E181D and E181D/Q329A for the first methylation are higher than that of the wild type, E181D and E181D/Q329A have the ability to add the second methyl group to the target mono-methyl arginine and generate ADMA and SDMA, respectively. The free energy barriers for E181D and E181D/Q329A to produce ADMA and SDMA, respectively, are considerably lower than the corresponding barriers involving the wild-type enzyme. Moreover, the computational study identifies some important structural, electronic and dynamic features that lead to the different product specificities and activities of the wild-type PRMT7, E181D and E181D/Q329A. These factors may play important roles in controlling the activity and product specificity of other PRMTs as well.

Key Words：Protein Arginine Methyltransferase; QM/MM molecular dynamics simulations; Free-energy simulations

# Introduction

It has been well established that protein, DNA and RNA methylations can play an important role in regulating biological activities.[1-6] The methylation processes are catalyzed by methyltransferases, and S-adenosyl-L-methionine (SAM) is often used as the methyl donor. Two of the best studied methylations of proteins are presumably lysine and arginine methylations which are catalyzed by protein lysine and arginine methyltransferases (PKMTs and PRMTs), respectively.[1,3] The biological consequences of lysine and arginine methylations (e.g., gene activation and repression) generally depend on the methylation states of the residues. Therefore, it is of considerable interest to determine why different methyltransferases may have different ability to direct specific degrees of methylation (named as product specificity). Such knowledge may also have important implications in developing strategies for manipulating signaling properties. Considerable efforts have been made to understand how product specificities are changed among PKMTs or PRMTs and to determine the structural and energetic origins of the product specificities.

Some important structural features and interactions at the active sites that control the product specificity of PKMTs have been identified. For instance, it has been observed that certain Tyr→Phe mutation (i.e., at the Tyr/Phe switch positions in the active sites) tends to increase the ability of PKMTs to add more methyl group(s) to the target lysine (if the residue is Tyr in wild-type), while the Phe→Tyr mutation tends to decrease this ability (if the residue is Phe in wild-type).[1,7-9] This effect of the Tyr/Phe switch has been well explained based on structural, biochemical and computational studies.[7-9] However, for PRMTs the methylation processes are more complex, and question remains concerning what are the factors that control the PRMT product specificity.[10,11] PRMTs have three different types based on the products they generated. Type I PRMTs catalyze the formation of the asymmetrically di-methylated arginine (ω-$N^G$, $N^G$-dimethylarginine or ADMA) with the two methyl groups attached to the same nitrogen $N^G$ atom,[12,13] while Type II PRMTs catalyze the formation of the symmetrically di-methylated arginine (ω-$N^G$, $N'^G$-dimethylarginine or SDMA) with each methyl group attached to one of the two nitrogen atoms ($N^G$ or $N'^G$).[14] PRMT7 to be studied in this work is the only member of Type III that generates mono-methylarginine (MMA) product.[15] MMA generated by PRMT7 represents a unique biological signal that is different from SDMA and ADMA. Recent experimental observations[16-18] of the changes of the PRMT7 activities as a result of certain mutations provide a unique opportunity for understanding the origin of the PRMT product specificity. Indeed, it has been shown that the E181D and E181D/Q329A mutants of PRMT7 can catalyze the formation of ADMA and SDMA, respectively,[16,17] while the F71I mutant can convert the enzyme into a mixed type I/II.[18] The ability of E181D and E181D/Q329A to add the second methyl at the specific positions is of considerably interest, and this may not be simply explained by the increase of the active site space as already shown from the earlier study of the F71 mutants.[18] Moreover, some other replacements from relatively large to relatively small residues either abolished the activity or did not lead to di-methylation of arginine. For instance, the formation of ADMA or SDMA was not observed for Q329A, W330A, E172D/E181D, E181D/I173G, E181D/W330A, E181D/Q329N, E181D/M75A and E181D/F71A for which one or two larger residues at the active site were replaced by smaller residues. Furthermore, it is not clear as to why E181D can only generate ADMA, while E181D/Q329A can only produce SDMA. Determination of the factors that lead to these changes of the product specificity may significantly enhance our understanding how the enzymes are able to fine-tune their specificities.

In our earlier comparative study of wild-type PRMT7 and E172Q, E181Q and Q329A mutants,[19] we showed that the activities followed the order of PRMT7 > Q329A > E181Q > E172Q, consistent with experimental observations. Moreover, PRMT7 was found to be only capable of generating MMA from the simulations. Through the comparison of structural and electronic properties for the reactions catalyzed by PRMT7 and its mutants, we identified three strategies of PRMT7 in reducing the activation barrier for the methyl transfer, including (1) formation of the reactive (near attack) conformations with the substrate Arg, (2) strengthening the active-site interactions at the transition state, and (3) generation of more effective nucleophiles by changing the charge distributions on the target Arg through the active-site interactions. It was demonstrated that it is a combination of these different factors that control the methylation activity of PRMT7 and these mutants. It would be of considerable interest to examine if some of these factors mentioned above would also play a role for changing the PRMT7's Type III product specificity as a result of the E181D and E181D/Q329A mutations.

In this work, QM/MM molecular dynamics and free energy (potential of mean force or PMF) simulations were carried out to study the activities and product specificities for E181D and E181D/Q329A. The simulations show that the free energy barriers of the E181D and E181D/Q329A mutants for the first methylation are about 1 and 2.5 kcal/mol higher, respectively, than that of the wild type PRMT7.[19] The results are consistent with experimental observations that E181D and E181D/Q329A have the ability to catalyze the formation of MMA with relatively lower activities and with the activity order of PRMT7 > E181D > E181D/Q329A.[16,17] For the second methylation, E181D was able to generate ADMA from MMA with a free energy barrier that is at least 4 kcal/mol lower compared to the barriers of the second methylation in the wild-type enzyme;[19] the barrier is also lower compared to that of generating SDMA in E181D. For E181D/Q329A, it was found that this double mutant was able to generate SDMA from MMA with a free energy barrier that is about 5-6 kcal/mol lower than that from wild type, while the barrier to produce ADMA in E181D/Q329A is as much as 10 kcal/mol higher compared to that of the SDMA formation. All these results are consistent with experimental observations concerning the activities and product specificity of the mutants. Analyses of the data generated from the simulations as well as Mullikan charge distributions provide rather useful information concerning the factors that control the product specificities and activities for PRMT7 and its mutants, and such information may have important implication for understanding the product specificity of PRMTs in general.

## Methods

The initial coordinates were based on a crystallographic complex of PRMT7 with S-adenosyl-L-homocysteine (SAH) and a histone H4 peptide (PDB ID: 4M38) containing the targeting Arg residue.[20] The methyl group was manually added to the $S_\delta$ of SAH to form a methyl donor SAM. The hydrogen atoms of this protein complex were added using the HBUILD module[21] in CHARMM. The initial structures for the entire stochastic boundary systems were optimized using the steepest descent (SD) and adopted-basis Newton−Raphson (ABNR) methods. The system was heated gradually from 50.0K to 298.15K in 50ps, and the equations of motion were integrated with a time step of 1fs. The coordinates were saved every 50 fs for analysis. The QM/MM MD and free energy (potential of mean force) simulations were carried out to determine the free energy profiles for the methyl transfer from SAM to the $N_{\eta1}$ or $N_{\eta2}$ atom of the target Arg/methyl Arg and to characterize the active site dynamics for the mutants (E181D and E181D/Q329A) of PRMT7 with the CHARMM program[22,23]. The −CH2−CH2−$S^+$(Me)−CH2− part of SAM, the side chains of the substrate arginine/methyl arginine and E172, D181 residues in E181D mutant (or E172, D181 and A329 in E181D/Q329A mutant) were treated by QM, and the rest of the system by MM. An all-hydrogen CHARMM potential function (PARAM27)[24] was applied for the MM region, and the self-consistent charge density functional tight-binding method (DFTB3)[25,26] was used for the QM region. The link-atom approach[27] implemented in CHARMM was used to separate the QM and MM region. An improved TIP3P water model[28] was used as the solvent.

Stochastic boundary molecular dynamics method[29] was used for the QM/MM MD and free energy simulations. The system was divided into a reaction zone and a reservoir zone, and the reaction zone was further divided into a reaction zone and a buffer zone. The reaction region is a sphere with radius r of 20 Å, and the buffer region has r in the range 20 Å $\leq$ r $\leq$ 22 Å. The reference center assigned by the system is located on the $N_{\eta2}$ atom on the substrate Arg/methyl Arg. The resulting system contains about 5,800 atoms, including about 480 water molecules. The QM/MM MD simulations of 1.5 ns were performed for the reactant complex of each methyl transfer reaction, and the distributions of r($C_M$−$N_{\eta 1/2}$) and θ were monitored. As discussed previously,[19] the $S_N2$ methyl transfer from SAM to arginine/methyl-arginine is presumably more efficient if the S−$CH_3$ group of SAM is well aligned with the lone pair of electrons on the $N_{\eta 1/2}$ atom of the target Arg/methyl Arg with a small θ (say, less than 30°) and a relatively short $C_M$−$N_{\eta 1/2}$ distance (say, about 3 Å)[30]. θ is defined as the angle between the direction of the $C_M$−$S_\delta$ bond ($r_2$) and the direction of the lone pair of electrons on the $N_{\eta 1/2}$ atom of Arg/methyl Arg ($r_1$) (Figure 1a). Another important structural parameter related to the efficiency of the methyl transfer is β($S_\delta$-$C_M \cdots N_{\eta 1/2}$) angle[31] which was also monitored in this work. The umbrella sampling method[32] and Weighted Histogram Analysis Method (WHAM)[33] were used to determine the changes in the free energy (potential of mean force or PMF) along the reaction coordinates of the methyl transfer from SAM to $N_{\eta 1}$ or $N_{\eta 2}$ of the target Arg/methyl Arg. The linear combination of r($C_M$−$N_{\eta 1/2}$) and r($C_M$−$S_\delta$) [R= r($C_M$−$S_\delta$) − r($C_M$−$N_{\eta 1/2}$)] was used as the reaction coordinate. For the methylation process, 22 to 25 simulation windows were performed, and for each window a production run of 100 ps was performed after 50 ps equilibration. The force constant of the harmonic biasing potentials used in the PMF simulations is 50−400 kcal $mol^{-1}$ $Å^{-2}$. For each system, five independent PMF simulations were performed. The free energies (PMFs) and statistical errors were taken, respectively, as the average values and standard deviations from the five runs. As it was pointed out in the earlier papers,[34] for the simple and similar $S_N2$ methyl transfer reactions such as those involving PRMT7 and its mutants studied here, the relative free energy barriers for the wild-type and mutated enzymes should be rather reliable due in part to the cancellation of errors. To study the effects of mutations on the charge distributions of the guanidine group, the Mulliken charge analyses were performed based on the DFTB3 calculations as used earlier;[19] the cluster models[19] of PRMT7 and the mutants were also constructed with the Mulliken charge analyses performed at the HF/STO-3G level using the Gaussian 03 suite of programs.[35]

## Results and discussion

### E181D mutant

The representative active-site structure of the reactant complex of E181D for the first methylation and r($C_M \cdots N_{\eta 1/2}$)/θ distribution maps (based on 1.5 ns QM/MM simulation) are plotted in Figure 1b. The average r($C_M$−$N_{\eta 1}$) and ($C_M$−$N_{\eta 2}$) distances between $C_M$ and $N_{\eta 1/2}$ of Arg are about 3.5 and 3.1Å, respectively, in the reactant complex. Consistent with the average distances, there is a large population of the structures with the relative short r($C_M$−$N_{\eta 2}$) distances (around 3.1 Å) and small values of the θ angle in the corresponding r-θ distribution map (i.e., the map on the right). The lone pair of electrons on $N_{\eta 2}$ (the atom designations for mono-methylation are given in Figure 1b) are better aligned with the methyl group of SAM, and therefore the methyl group is likely to transfer to $N_{\eta 2}$ rather than to $N_{\eta 1}$.[19] The average structure in Figure 1b shows that while the salt bridge between E172 and Arg is similar to what was observed in the wild-type enzyme complex,[19] the interaction between D181 and Arg is somewhat different from that involving E181. Indeed, only one of the carboxylate oxygen from D181 interacts with Arg, presumably due to the shortening of the sidechain in going from E181 to D181. Nevertheless, the interaction between D181 and Arg is quite strong. One of the obvious structural effects from the mutation is the change of the relative orientation of the transferable methyl group from SAM and target Arg. Figure 1c shows that while the β($S_\delta$-$C_M \cdots N_{\eta 2}$) angle can reach to 160-180° in the wild-type enzyme with a significant population, it cannot do so in E181D. Since β($S_\delta$-$C_M \cdots N_{\eta 2}$) needs to be close to 180° for the effective electronic overlap during the bond formation between $C_M$ and $N_{\eta 2}$, the activity of E181D is expected to be reduced as a result. Consistent with this suggestion, experimental results[16,17] showed that the activity of E181D was considerably lower compared to wild-type. Our previous study[19] also demonstrated that one of the possible roles of E181 is to reduce the positive charge on Arg and make its attack on the positively charged methyl group of SAM energetically more favorable. The Mulliken charge analysis given in Table S1 in Supporting Information shows that there is an increase of the positive charge on the ω-guanidino group as a result of E181→D mutation, suggesting that D181 is less effective in this regard; this may contribute to the reduction of the activity as well.

The free energy profiles for the methyl addition to $N_{\eta2}$ are given in Figure 1d and 1f for the cases of the proton transfer to E172 and D181, respectively. The free energy barriers are similar in the two cases; the similar observation was also made in some cases in the earlier study.[19] The free energy barriers for the mono-methylation in E181D are higher than that obtained for wild-type,[19] consistent with the discussion above and experimental observations.[16,17] The free energy simulations were also performed for the methyl transfer to $N_{\eta1}$. However, the free energy barrier is considerably higher compared to those given in Figure 1d and 1f (see Figure S2). The active site structures near transition state (TS) are given in Figure 1e and 1g for the cases of proton transfer to E172 and D181 during the methylation, respective. As can be seen from these figures, the proton transfer has not occurred at the TS; the proton transfer occurred about three windows after passing the TS in the free energy simulations and these structures are given in Figure S2. Comparison of the structures in Figure 1e and 1g with that in Figure 1b shows that the average distances for the salt bridge interactions between the substrate Arg and E172/D181 decreases from 3.0 to 2.8 Å in going from the reactant complex to near TS, suggesting that the corresponding interactions become stronger at the TS. Strengthening such interactions in going from the reactant state to the TS is expected to contribute to the transition state stabilization for E181D; the similar observation has been made for the wild-type enzyme as well.[19]

Although PRMT7 is Type III PRMT that catalyzes the formation of mono-methylarginine (MMA) product, recent experimental studies[16,17] demonstrated that when an already methylated H4 peptide at Arg3 ($H4^{1-21}$R3MMA) was used as a substrate, the E181D mutant was able to catalyze the formation of ADMA. Since the crystal structure of E181D in complex with $H4^{1-21}$R3MMA is not available, we tested the formation of ADMA or SDMA in E181D using QM/MM MD and free energy simulations with a variety of the possible initial MMA configurations in the mutant (see Table S2). The average structure of the reactant complex that led to the lowest free energy barriers is given in Figure 2a along with $r(C_M\cdots N_{\eta1/2})/\theta$ and $\beta(S_\delta\text{-}C_M\cdots N_{\eta1/2})$ distribution maps. For the second methylation, $N_{\eta2}$ is designated as the nitrogen atom that has already been mono-methylated. Similar to the case for the first methyl transfer, only one of the carboxylate oxygen from D181 interacts strongly with methyl Arg in the reactant complex. It is of interest to note from Figure 2a that the transferable methyl group is closer to the nitrogen that already has a methyl group on it (i.e., $N_{\eta2}$). Moreover, the $\beta(S_{\delta}\text{-}C_{M}\cdots N_{\eta2})$ angle is also more favorable for the methyl transfer to $N_{\eta2}$. One of the reasons for the formation of such configuration is probably due to the steric repulsions between the methyl group on MMA and some of the active site residues (e.g., Q329) that change the relative positions of the transferable methyl group and methyl Arg. Consistent with this observation, the free energy barrier for the methyl transfer to $N_{\eta2}$ with the proton transfers to E172 is lower than those to $N_{\eta1}$ (see Figure 2b and 2d); however, the barrier for the methyl transfer to $N_{\eta1}$ with the proton transfers to D181 is much higher. Moreover, the free energy barrier for the methyl transfer to $N_{\eta2}$ in E181D is also considerably lower (by as much 5-10 kcal/mol) than the all barriers obtained in the wild-type enzyme for the second methyl transfer.[19] Thus, the results of the QM/MM MD and free energy simulations suggest that the possibility for di-methylation in the E181D mutant is significantly higher than in wild-type and the di-methylation product is likely to be ADMA rather than SDMA, consistent with experimental observation.[16,17]

**E181D/Q329A mutant**

The representative active-site structure of the reactant complex of E181D/Q329A for the first methylation and $r(C_{M}\cdots N_{\eta1/2})/\theta$ distribution maps are plotted in Figure 3a. The average $r(C_{M}\text{–}N_{\eta1})$ and $(C_{M}\text{–}N_{\eta2})$ distances between $C_{M}$ and $N_{\eta1/2}$ of Arg are about 3.5 and 3.1Å, respectively, in the reactant complex. Figure 3a also shows that there is a large population of the structures with the relative short $r(C_{M}\text{–}N_{\eta2})$ distances (around 3.1 Å) and small values of the $\theta$ angle in the corresponding r-$\theta$ distribution map. Moreover, the $\beta(S_{\delta}\text{-}C_{M}\cdots N_{\eta1/2})$ distribution maps (Figure S3a) show that the both $\beta(S_{\delta}\text{-}C_{M}\cdots N_{\eta1})$ and $\beta(S_{\delta}\text{-}C_{M}\cdots N_{\eta2})$ angles can reach to 160-180° in E181D/Q329A. Therefore, the lone pair of electrons on $N_{\eta2}$ are better aligned with the methyl group of SAM, and the methyl group is likely to transfer to $N_{\eta2}$ rather than to $N_{\eta1}$. Consistent with this suggestion, the free energy barrier for the first methyl transfer to $N_{\eta2}$ (Figure

3b) is considerably lower than that for the first methyl transfer to $N_{\eta 1}$ (Figure S3b); in the both cases only the proton transfer to E172 was observed. The average structure near TS is plotted in Figure 3c. As in the earlier cases, strengthening salt bridge interactions involving E172 and D181 in going from the reactant state to the TS is observed. The Mulliken charge analysis (Table S1) shows that there also is an increase of the positive charge on the ω-guanidino group as a result of E181→D/Q329→A double mutation, and this may contribute to the reduction of the activity.

The average structure of the reactant complex of the 2nd methylation in E181D/Q329A is given in Figure 4a along with $r(C_M \cdots N_{\eta 1/2})/\theta$ distribution maps. As before, for the second methylation $N_{\eta 2}$ is designated as the nitrogen atom that has already been mono-methylated. It is of interest to see from Figure 4a that the transferable methyl group is now well aligned with $N_{\eta 1}$. Indeed, the average $r(C_M \cdots N_{\eta 1})$ distance is about 3.2Å, while $r(C_M \cdots N_{\eta 2})$ is about 3.8Å. Thus, the second methyl group is likely to transfer to $N_{\eta 1}$ rather than to $N_{\eta 2}$, leading to SDMA. One of the reasons for the formation of this configuration favoring SDMA is probably due to the removal of the steric repulsions between the methyl group on MMA and Q329 as a result of the Q329A mutation, and this allows the methyl Arg to occupy the position favorable for SDMA. Consistent with the structural and dynamic analysis, the free energy profiles show that the barriers for the formation of SDMA (Figure 4b) are significantly lower than the barrier of the formation of ADMA (Figure 4d) as well as some other barriers (see Table S4). Some important bond distances in the active site of the reaction state and transition state for the 2nd methylation in E181D, E181D/Q329A and wild type of PRMT7 are given in Table S3.

## Conclusion

Question remains concerning why different PRMTs may generate different methylation states for the target arginine residues on protein substrates. It has been observed[16,17] that the E181D and E181D/Q329A mutants of PRMT7 of Type III can catalyze the formation of ADMA and SDMA, respectively. Thus, E181D has the product specificity property of Type I PRMTs, while E181D/Q329A has the product specificity property of Type II PRMTs. The exact reasons as to why the mutants have such abilities are not clear. In this work, QM/MM MD and free energy (PMF) simulations have been performed to understand the origin of the product specificity changes. The free energy profiles for the formation of ADMA and SDMA from MMA in wild-type enzyme, E181D and E181D/Q329A are summarized in Figure 5. Figure 5a shows that for the formation of ADMA the free energy barriers for the second methyl transfer in the wild-type PRMT7 and E181D/Q329A are more than 8 kcal/mol higher than that in E181D, suggesting that ADMA can only be formed in E181D. Figure 5b shows that for the formation of SDMA the free energy barriers for the second methyl transfer in the wild-type PRMT7 and E181D are more than 5 kcal/mol higher than that in E181D/Q329A. Thus, only E181D/Q329A can produce SDMA. The structural, dynamic and Mulliken charge analysis have been performed, and it was found that the ability of the reactant complexes to form the good reactive, near attack configuration seems to be a key factor. The simulation results make it possible to explain the changes of the product specificity properties for the two mutants, and such information may have important implications for understanding the product specificity of PRMTs in general.

## Acknowledgments

We thank Professor Martin Karplus for a gift of the CHARMM program. This work was supported by the Natural Science Foundation of China (No. 22177064 to P.Q.) and the Natural Science Foundation of Shandong Province (No. ZR2017MB048 to P.Q.).

# References

(1) Cheng, X.; Collins, R. E.; Zhang, X. *Annual Review of Biophysics and Biomolecular Structure* **2005**, *34*, 267.

(2) Greer, E. L.; Shi, Y. *Nature Reviews Genetics* **2012**, *13*, 343.

(3) Blanc, R. S.; Richard, S. *Molecular Cell* **2017**, *65*, 8.

(4) Guccione, E.; Richard, S. *Nature Reviews Molecular Cell Biology* **2019**, *20*, 642.

(5) Shi, H. L.; Wei, J. B.; He, C. *Molecular Cell* **2019**, *74*, 640.

(6) Zaccara, S.; Ries, R. J.; Jaffrey, S. R. *Nature Reviews Molecular Cell Biology* **2019**, *20*, 608.

(7) Couture, J. F.; Dirk, L. M. A.; Brunzelle, J. S.; Houtz, R. L.; Trievel, R. C. *Proceedings of the National Academy of Sciences of the United States of America* **2008**, *105*, 20659.

(8) Yao, J. Z.; Chu, Y. Z.; An, R.; Guo, H. *Journal of Chemical Information and Modeling* **2012**, *52*, 449.

(9) Xu, Q.; Chu, Y. Z.; Guo, H. B.; Smith, J. C.; Guo, H. *Chemistry-a European Journal* **2009**, *15*, 12596.

(10) Zhang, X.; Cheng, X. *Structure* **2003**, *11*, 509.

(11) Sun, L.; Wang, M.; Lv, Z.; Yang, N.; Liu, Y.; Bao, S.; Gong, W.; Xu, R.-M. *Proceedings of the National Academy of Sciences* **2011**, *108*, 20538.

(12) Lee, W.-C.; Lin, W.-L.; Matsui, T.; Chen, E. S. W.; Wei, T.-Y. W.; Lin, W.-H.; Hu, H.; Zheng, Y. G.; Tsai, M.-D.; Ho, M.-C. *Biochemistry* **2015**, *54*, 7514.

(13) Bonnefond, L.; Stojko, J.; Mailliot, J.; Troffer-Charlier, N.; Cura, V.; Wurtz, J.-M.; Cianférani, S.; Cavarelli, J. *Journal of Structural Biology* **2015**, *191*, 175.

(14) Yang, Y.; Hadjikyriacou, A.; Xia, Z.; Gayatri, S.; Kim, D.; Zurita-Lopez, C.; Kelly, R.; Guo, A.; Li, W.; Clarke, S. G.; Bedford, M. T. *Nature Communications* **2015**, *6*, 6428.

(15) Zurita-Lopez, C. I.; Sandberg, T.; Kelly, R.; Clarke, S. G. *Journal of Biological Chemistry* **2012**, *287*, 7859.

(16) Jain, K.; Warmack, R. A.; Debler, E. W.; Hadjikyriacou, A.; Stavropoulos, P.; Clarke, S. G. *Journal of Biological Chemistry* **2016**, *291*, 18299.

(17) Debler, E. W.; Jain, K.; Warmack, R. A.; Feng, Y.; Clarke, S. G.; Blobel, G.; Stavropoulos, P. *Proceedings of the National Academy of Sciences of the United States of America* **2016**, *113*, 2068.

(18) Caceres, T. B.; Thakur, A.; Price, O. M.; Ippolito, N.; Li, J.; Qu, J.; Acevedo, O.; Hevel, J. M. *Biochemistry* **2018**, *57*, 1349.

(19) Ren, W. S.; Jiang, K. B.; Deng, H.; Lu, N.; Yu, T.; Guo, H.; Qian, P. *J Chem Theory Comput* **2020**, *16*, 5301.

(20) Wang, C.; Zhu, Y.; Caceres, Tamar B.; Liu, L.; Peng, J.; Wang, J.; Chen, J.; Chen, X.; Zhang, Z.; Zuo, X.; Gong, Q.; Teng, M.; Hevel, Joan M.; Wu, J.; Shi, Y. *Structure* **2014**, *22*, 756.

(21) Brünger, A. T.; Karplus, M. *Proteins: Structure, Function, and Genetics* **1988**, *4*, 148.

(22) Brooks, B. R.; Brooks, C. L.; Mackerell, A. D.; Nilsson, L.; Petrella, R. J.; Roux, B.; Won, Y.; Archontis, G.; Bartels, C.; Boresch, S.; Caflisch, A.; Caves, L.; Cui, Q.; Dinner, A. R.; Feig, M.; Fischer, S.; Gao, J.; Hodoscek, M.; Im, W.; Kuczera, K.; Lazaridis, T.; Ma, J.; Ovchinnikov, V.; Paci, E.; Pastor, R. W.; Post, C. B.; Pu, J. Z.; Schaefer, M.; Tidor, B.; Venable, R. M.; Woodcock, H. L.; Wu, X.; Yang, W.; York, D. M.; Karplus, M. *Journal of Computational Chemistry* **2009**, *30*, 1545.

(23) Brooks, B. R.; Bruccoleri, R. E.; Olafson, B. D.; States, D. J.; Swaminathan, S.; Karplus, M. *Journal of Computational Chemistry* **1983**, *4*, 187.

(24) MacKerell, A. D.; Bashford, D.; Bellott, M.; Dunbrack, R. L.; Evanseck, J. D.; Field, M. J.; Fischer, S.; Gao, J.; Guo, H.; Ha, S.; Joseph-McCarthy, D.; Kuchnir, L.; Kuczera, K.; Lau, F. T. K.; Mattos, C.; Michnick, S.; Ngo, T.; Nguyen, D. T.; Prodhom, B.; Reiher, W. E.; Roux, B.; Schlenkrich, M.; Smith, J. C.; Stote, R.; Straub, J.; Watanabe, M.; Wiórkiewicz-Kuczera, J.; Yin, D.; Karplus, M. *The Journal of Physical Chemistry B* **1998**, *102*, 3586.

(25) Cui, Q.; Elstner, M.; Kaxiras, E.; Frauenheim, T.; Karplus, M. *The Journal of Physical Chemistry B* **2001**, *105*, 569.

(26) Elstner, M.; Porezag, D.; Jungnickel, G.; Elsner, J.; Haugk, M.; Frauenheim, T.; Suhai, S.; Seifert, G. *Physical Review B* **1998**, *58*, 7260.

(27) Field, M., J. ; Bash, P., A. ; Karplus, M. *Journal of Computational Chemistry* **1990**, *11*, 700.

(28) Jorgensen, W. L.; Chandrasekhar, J.; Madura, J. D. *The Journal of Chemical Physics* **1983**, *79*, 926.

(29) Brooks III, C. L.; Brünger, A.; Karplus, M. *Biopolymers* **1985**, *24*, 843.

(30) Chu, Y.; Xu, Q.; Guo, H. *Journal of Chemical Theory and Computation* **2010**, *6*, 1380.

(31) Zhang, X. D.; Bruice, T. C. *Biochemistry* **2008**, *47*, 6671.

(32) Torrie, G. M.; Valleau, J. P. *Chemical Physics Letters* **1974**, *28*, 578.

(33) Kumar, S.; Rosenberg, J. M.; Bouzida, D.; Swendsen, R. H.; Kollman, P. A. *Journal of Computational Chemistry* **1992**, *13*, 1011.

(34) Deng, H.; Ma, Y.; Ren, W.-S.; Vuong, V. Q.; Qian, P.; Guo, H. *ACS Catalysis* **2020**, *10*, 13314.

(35) Schlegel, H.; Scuseria, G.; Robb, M.; Cheeseman, J.; Montgomery Jr, J.; Vreven, T.; Kudin, K.; Burant, J.; Millam, J.; Iyengar, S. *Gaussian, Inc.: Wallingford, CT* **2004**.

# Figure Caption

**Figure 1.** Results for the first methylation in E181D. Only the results for the methyl transfer to $N_{\eta2}$ are given, as the free energy barrier for the methyl transfer to $N_{\eta1}$ is too high (see Figure S1). (a) Relative orientation of SAM and Peptidyl-Arg in the reactant complex. $\theta$ is defined as the angle between the two vectors $r_1$ and $r_2$. Here, $r_1$ is the direction of the lone pair of electrons on the $N_{\eta1}$ or $N_{\eta2}$ atom, and $r_2$ is the vector pointing from $C_M$ to $S_\delta$. (b) The reactant complex for the 1st methylation containing SAM (methyl donor) and the substrate Arg along with $r(C_M\text{-}N_{\eta1/2})$ and $\theta$ distributions obtained from the QM/MM MD simulations of the E181D mutant (left: the distribution map for $N_{\eta1}$; right: the distribution map for $N_{\eta2}$). The average values of some distances are also given. (c) $r(C_M\text{-}N_{\eta2})$ and $\beta(S_\delta\text{-}C_M\cdots N_{\eta2})$ distributions for wild-type PRMT7 and E181D. (d) Free energy (PMF) profile for the 1st methyl transfer to $N_{\eta2}$ as a function of the reaction coordinate $[R = r(C_M{-}S_\delta) - r(C_M{-}N_{\eta2})]$ that is accompanied by proton transfer to the carboxylate group of E172. The value of the reaction coordinate X at TS and the free energy barrier Y are also listed as (X, Y). (e) A representative active site structure of near TS of Figure 1c. (f) PMF profile and (g) a representative active-site structure of near TS for the 1st methyl transfer to $N_{\eta2}$ that is accompanied by proton transfer to the carboxylate group of D181.

**Figure 2.** Results for the second methylation in E181D. Only the substrate configuration with the methyl group of the mono-methyl arginine located near Q329 is considered here, as the rest three configurations have either very high free energy barrier for methyl transfer or unstable during dynamics (see Table S2). The monomethylated nitrogen atom is designated as $N_{\eta2}$ for the second methylation. (a) A representative active site structure of the reactant complex for the 2nd methylation along with some average distances and $r(C_M\text{-}N_{\eta1/2})$ and the distributions maps obtained from the QM/MM dynamics simulations. (b) Free energy PMF profile and (c) a representative active-site structure of near TS for the 2nd methyl transfer to $N_{\eta2}$ that is accompanied by proton transfer to the carboxylate group of E172. The value of the reaction coordinate X at TS and the free energy barrier Y are also list as (X, Y) for the free energy profile. (d) Free energy PMF profile for the 2nd methyl transfer to $N_{\eta1}$ as well as the proton transfer to E172 (top) or to D181 (bottom). (e) A representative active-site structure of near TS for the 2nd methyl transfer to $N_{\eta1}$ and proton transfer to E172; the corresponding structure for proton transfer to D181 is given in Supporting Information (Figure S10).

**Figure 3.** Results for the first methylation for E181D/Q329A. Only the results for the

methyl transfer to $N_{\eta 2}$ are given, as the free energy barrier for the methyl transfer to $N_{\eta 1}$ is much higher (Figure S3). (a) The reactant complex for the 1st methylation containing SAM (methyl donor) and the substrate Arg along with $r(C_M\text{-}N_{\eta 1/2})$ and $\theta$ distributions obtained from the QM/MM MD simulations of the E181D/Q329A mutant (left: the distribution map for $N_{\eta 1}$; right: the distribution map for $N_{\eta 2}$). The average values of some distances are also given. (b) Free energy (PMF) profile for the 1st methyl transfer to $N_{\eta 2}$ as a function of the reaction coordinate $[R = r(C_M{-}S_\delta) - r(C_M{-}N_{\eta 2})]$ that is accompanied by proton transfer to the carboxylate group of E172. (c) A representative active site structure of near TS of Figure 3b.

**Figure 4.** Results for the second methylation for E181D/Q329A. Only the substrate configuration with the methyl group of the mono-methyl arginine located near A329 is considered here, as the rest three configurations have either much higher free energy barriers for methyl transfer (see Table S4). (a) A representative active site structure of the reactant complex for the 2nd methylation along with some average distances and $r(C_M\text{-}N_{\eta 1/2})$ and $\theta$ distributions obtained from the QM/MM dynamics simulations. (b) Free energy PMF profile for the 2nd methyl transfer to $N_{\eta 1}$ as well as the proton transfer to E172 (top) or to D181 (bottom). (c) A representative active-site structure of near TS for the 2nd methyl transfer to $N_{\eta 1}$ and proton transfer to E172. (d) Free energy PMF profile and (e) a representative active-site structure of near TS for the 2nd methyl transfer to $N_{\eta 2}$ that is accompanied by proton transfer to the carboxylate group of E172.

**Figure 5.** Comparison of the free energy profiles for the formation of ADMA and SDMA from MMA in wild-type enzyme, E181D and E181D/Q329A. The value of the reaction coordinate X at TS and the free energy barrier Y are also list as (X, Y) in each case. (a) The ADMA methylation in wild-type enzyme, E181D and E181D/Q329A. (b) The SDMA methylation in wild-type enzyme, E181D and E181D/Q329A.

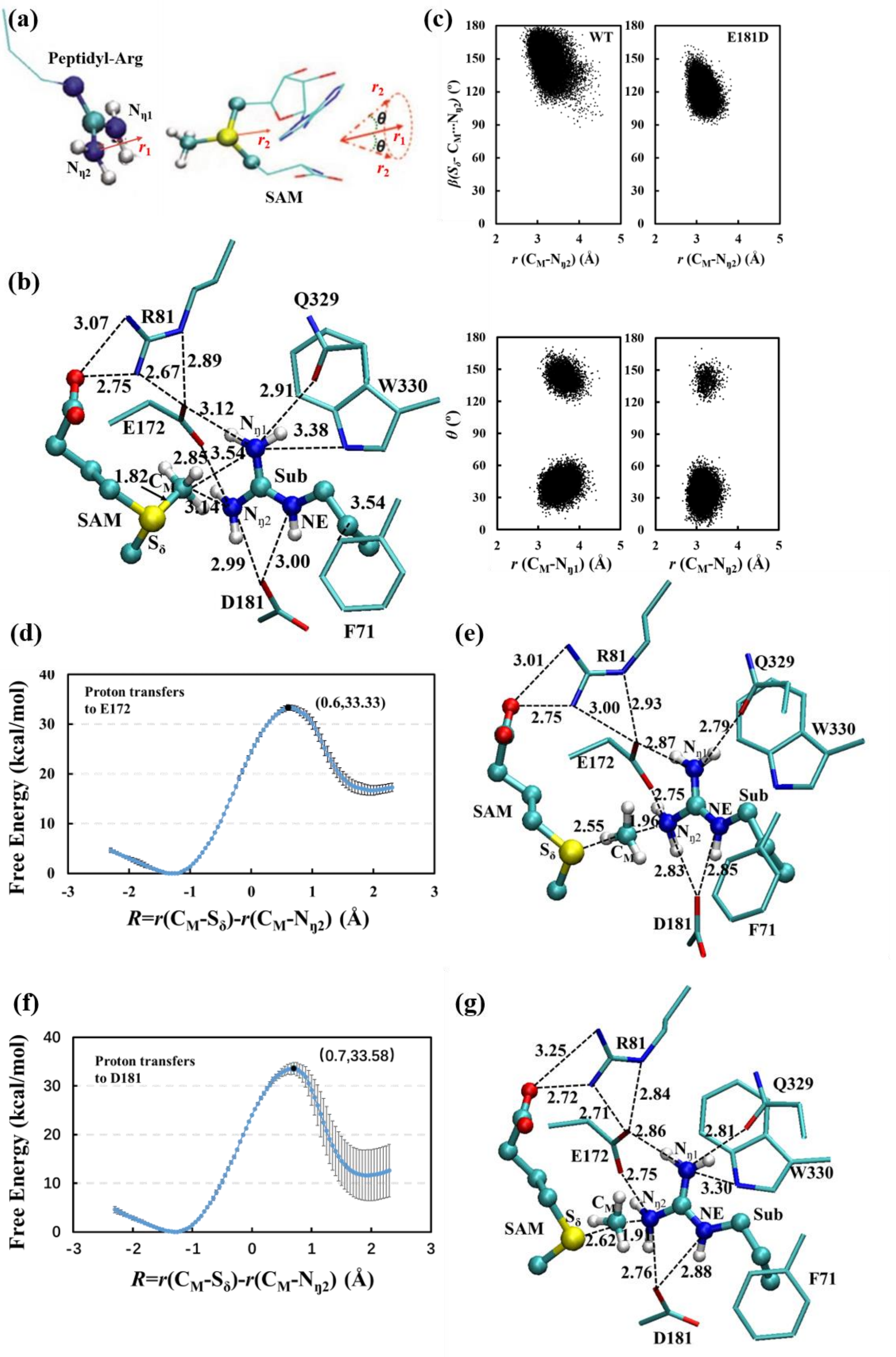
(a)
Peptidyl-Arg
Nη1
Nη2
r1
r2
SAM
θ
(c)
WT
E181D
β(Sδ- CM···Nη2) (°)
r (CM-Nη2) (Å)
θ (°)
r (CM-Nη1) (Å)
(b)
3.07
R81
2.89
2.67
2.75
Q329
2.91
W330
3.12
E172
Nη1
3.38
3.54
2.85
1.82
CM
Sub
3.54
3.14
Nη2
NE
SAM
Sδ
2.99
3.00
D181
F71
(d)
Proton transfers to E172
(0.6,33.33)
Free Energy (kcal/mol)
R=r(CM-Sδ)-r(CM-Nη2) (Å)
(e)
3.01
R81
2.75
3.00
2.93
Q329
2.79
W330
E172
2.87
Nη1
2.75
NE
Sub
SAM
2.55
1.96
Nη2
Sδ
CM
2.83
2.85
D181
F71
(f)
Proton transfers to D181
(0.7,33.58)
Free Energy (kcal/mol)
R=r(CM-Sδ)-r(CM-Nη2) (Å)
(g)
3.25
R81
2.72
2.84
2.71
2.86
Q329
2.81
E172
Nη1
2.75
W330
3.30
CM
Nη2
NE
Sub
SAM
Sδ
2.62
1.91
2.76
2.88
F71
D181

**Figure 1**

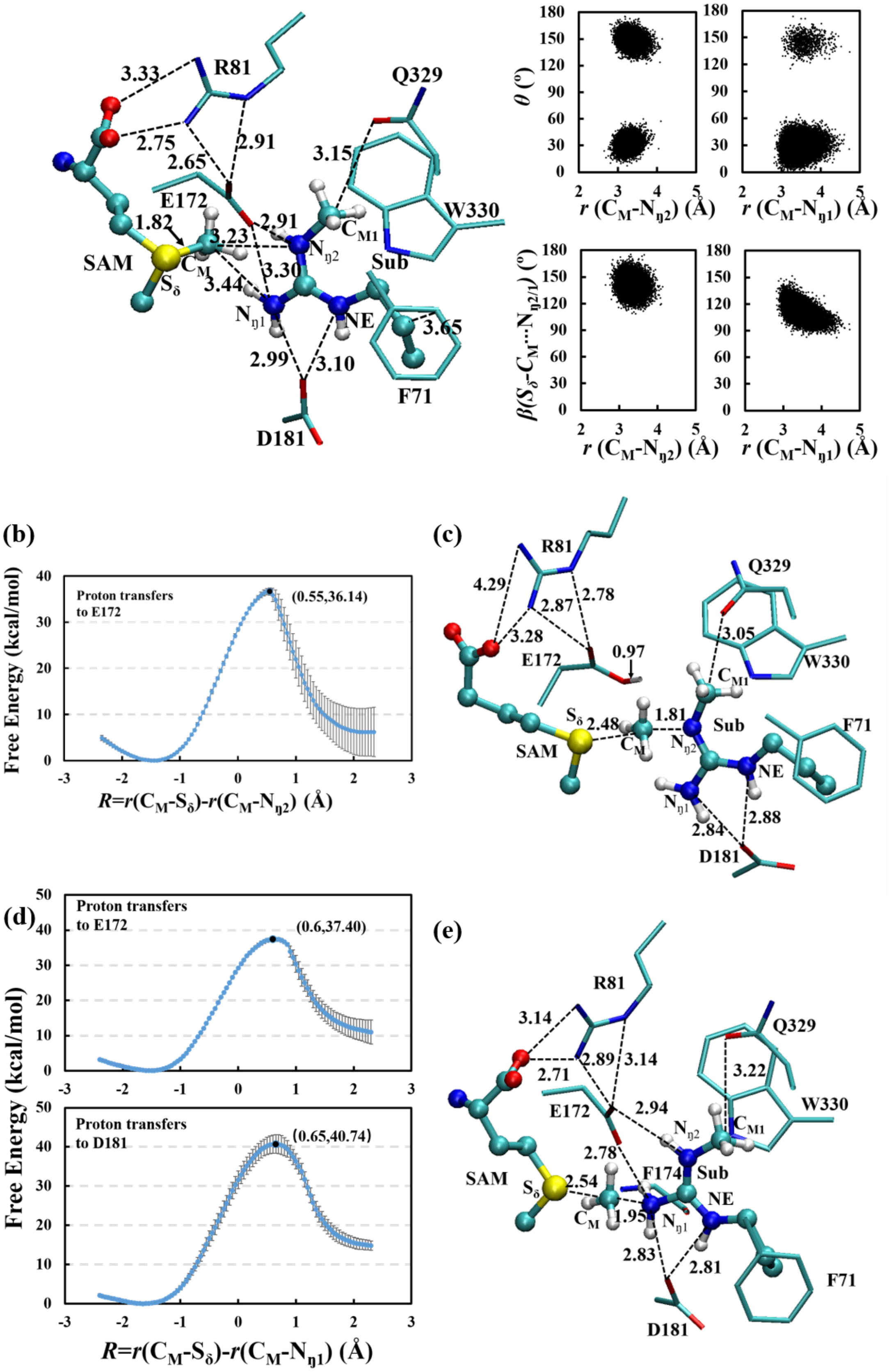
3.33
R81
2.75
2.65
2.91
Q329
3.15
E172
2.91
CM1
W330
1.82
SAM
3.23
Nη2
CM
Sub
Sδ
3.30
3.44
Nη1
NE
3.65
2.99
3.10
F71
D181
θ (°)
r (CM-Nη2) (Å)
r (CM-Nη1) (Å)
β(Sδ-CM···Nη2/1) (°)
180
150
120
90
60
30
0
2
3
4
5
(b)
Proton transfers to E172
(0.55,36.14)
Free Energy (kcal/mol)
R=r(CM-Sδ)-r(CM-Nη2) (Å)
40
30
20
10
0
-3
-2
-1
0
1
2
3
(c)
R81
4.29
2.87
2.78
Q329
3.28
E172
0.97
3.05
W330
CM1
Sδ
2.48
1.81
SAM
CM
Nη2
Sub
F71
NE
Nη1
2.84
2.88
D181
(d)
Proton transfers to E172
(0.6,37.40)
Proton transfers to D181
(0.65,40.74)
Free Energy (kcal/mol)
R=r(CM-Sδ)-r(CM-Nη1) (Å)
50
40
30
20
10
0
-3
-2
-1
0
1
2
3
(e)
R81
3.14
2.71
2.89
3.14
Q329
3.22
E172
2.94
W330
Nη2
CM1
2.78
SAM
F174
Sub
Sδ
2.54
NE
CM
1.95
Nη1
2.83
2.81
F71
D181

Figure 2

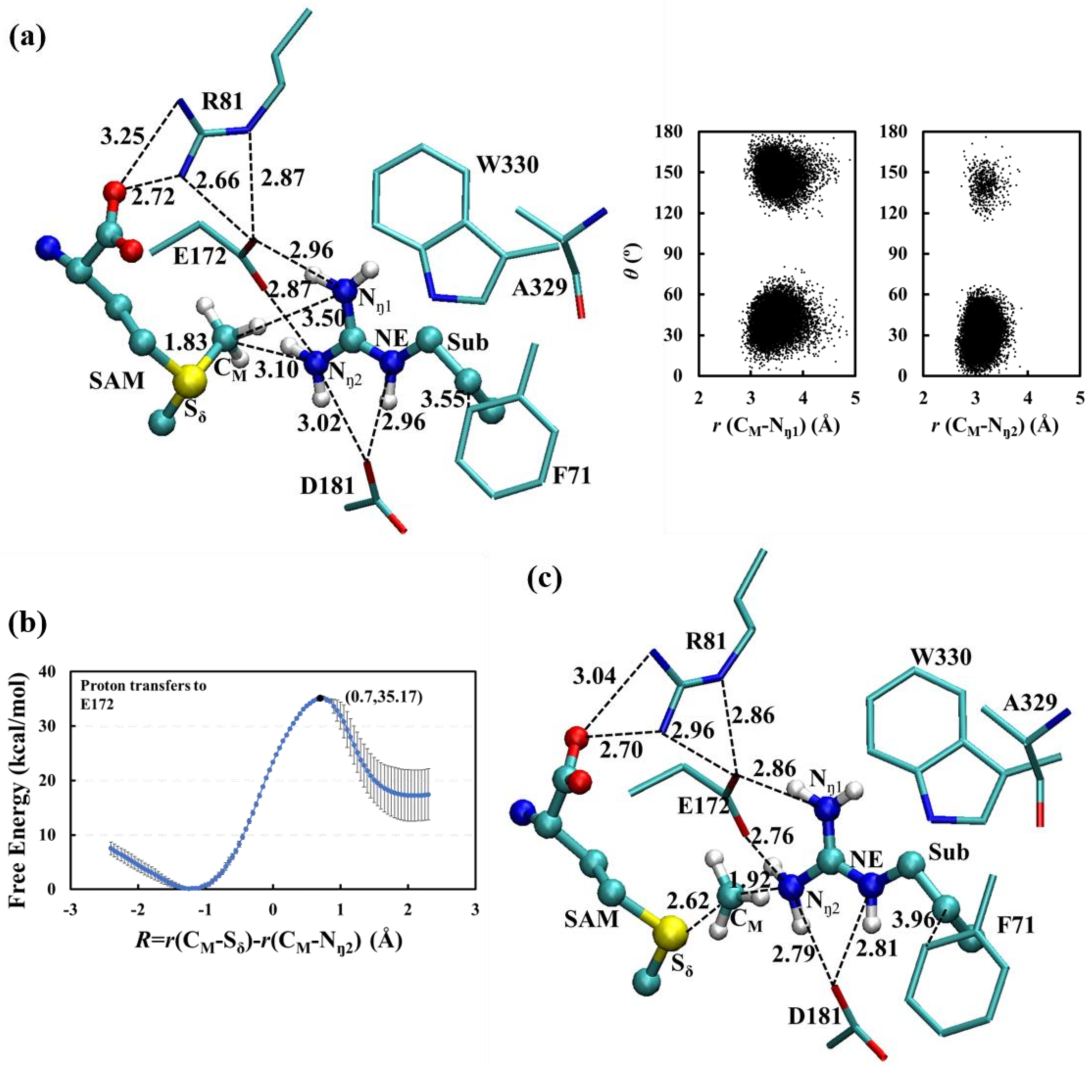
(a)
R81
3.25
2.72
2.66
2.87
W330
E172
2.96
2.87
N_η1
3.50
A329
1.83
NE
Sub
SAM
C_M
3.10
N_η2
S_δ
3.02
2.96
3.55
D181
F71
180
150
120
90
60
30
0
θ (°)
2
3
4
5
r (C_M-N_η1) (Å)
r (C_M-N_η2) (Å)
(b)
Free Energy (kcal/mol)
40
30
20
10
0
Proton transfers to E172
(0.7,35.17)
-3
-2
-1
0
1
2
3
R=r(C_M-S_δ)-r(C_M-N_η2) (Å)
(c)
R81
3.04
W330
2.70
2.96
2.86
A329
2.86
N_η1
E172
2.76
1.92
NE
Sub
SAM
2.62
C_M
N_η2
3.96
F71
S_δ
2.79
2.81
D181

Figure 3

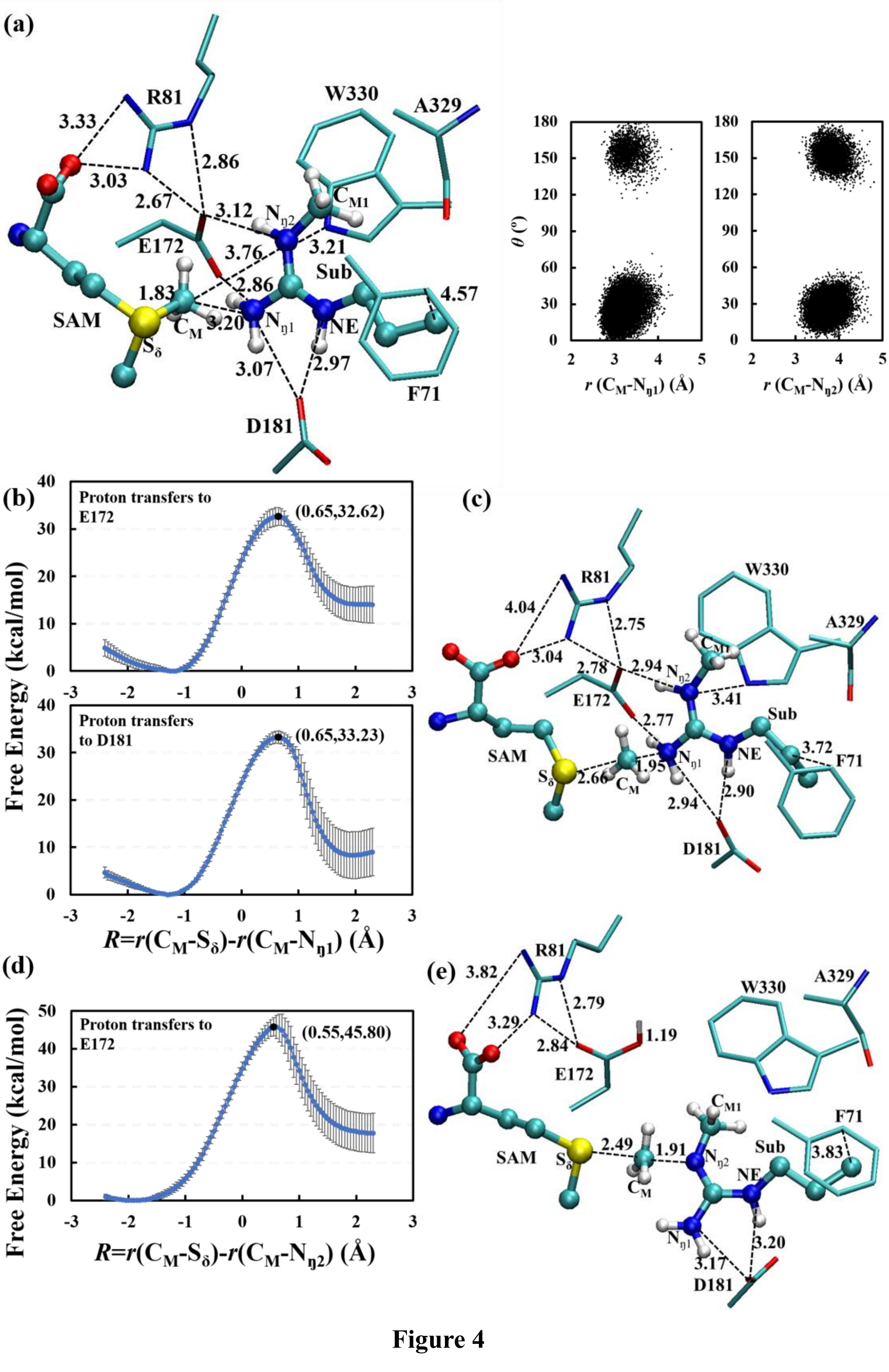
(a)
R81
W330
A329
3.33
3.03
2.86
2.67
3.12
$N_{\eta2}$
$C_{M1}$
E172
3.76
3.21
Sub
1.83
2.86
4.57
SAM
$C_M$
3.20
$N_{\eta1}$
NE
$S_\delta$
3.07
2.97
F71
D181
180
150
120
90
60
30
0
$\theta$ (°)
2
3
4
5
$r$ ($C_M$-$N_{\eta1}$) (Å)
$r$ ($C_M$-$N_{\eta2}$) (Å)
(b)
Proton transfers to E172
(0.65,32.62)
Proton transfers to D181
(0.65,33.23)
Free Energy (kcal/mol)
40
30
20
10
0
-3
-2
-1
0
1
2
3
$R=r(C_M-S_\delta)-r(C_M-N_{\eta1})$ (Å)
(c)
R81
W330
4.04
2.75
A329
$C_{M1}$
3.04
2.78
2.94
$N_{\eta2}$
3.41
E172
Sub
2.77
SAM
$S_\delta$
2.66
$C_M$
1.95
$N_{\eta1}$
NE
3.72
F71
2.94
2.90
D181
(d)
Proton transfers to E172
(0.55,45.80)
Free Energy (kcal/mol)
50
40
30
20
10
0
-3
-2
-1
0
1
2
3
$R=r(C_M-S_\delta)-r(C_M-N_{\eta2})$ (Å)
(e)
3.82
R81
2.79
W330
A329
3.29
2.84
1.19
E172
F71
$C_{M1}$
SAM
$S_\delta$
2.49
1.91
$N_{\eta2}$
Sub
3.83
NE
$C_M$
$N_{\eta1}$
3.20
3.17
D181

Figure 4

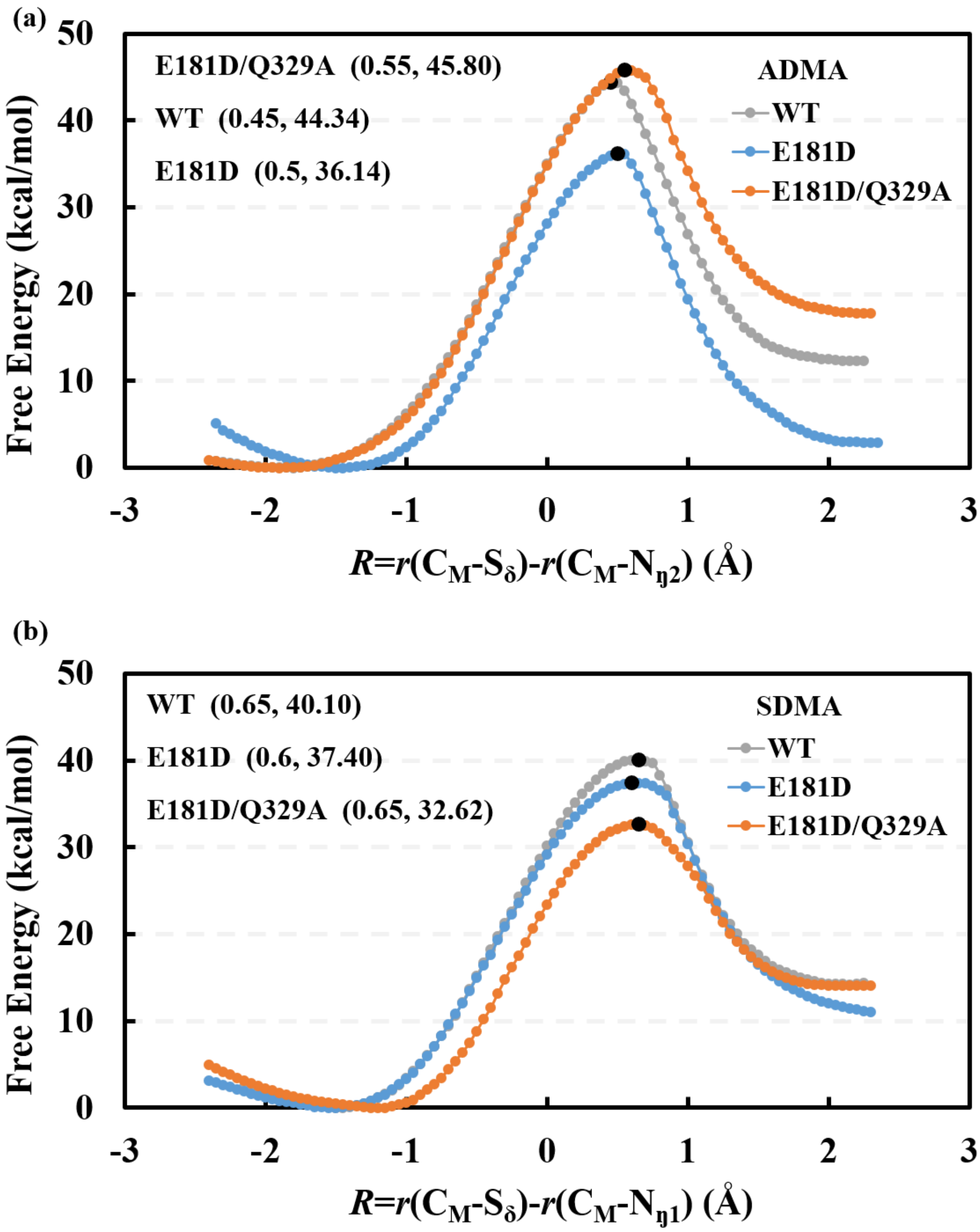
(a)
Free Energy (kcal/mol)
50
40
30
20
10
0
E181D/Q329A (0.55, 45.80)
WT (0.45, 44.34)
E181D (0.5, 36.14)
ADMA
WT
E181D
E181D/Q329A
-3
-2
-1
0
1
2
3
R=r(C_M-S_δ)-r(C_M-N_η2) (Å)
(b)
Free Energy (kcal/mol)
50
40
30
20
10
0
WT (0.65, 40.10)
E181D (0.6, 37.40)
E181D/Q329A (0.65, 32.62)
SDMA
WT
E181D
E181D/Q329A
-3
-2
-1
0
1
2
3
R=r(C_M-S_δ)-r(C_M-N_η1) (Å)

**Figure 5**